DIELECTROPHORETIC-ASSISTED BIOSENSOR FOR SINGLE-CELL CHARACTERIZATION AT MMWAVE FREQUENCIES IN CMOS 28NM TECHNOLOGY

Ali Ameri[1], Luya Zhang[1], Asmaysinh Gharia[1,2], Mekhail Anwar[2], and Ali M. Niknejad[1*]*
[1] University of California, Berkeley, CA, USA and
[2] University of California, San Francisco, CA, USA.
[*]Authors contributed equally to this work.

ABSTRACT

In this work an on-chip solution for integrating Dielectrophoretic (DEP) single cell manipulation and mmWave permittivity sensing in a low-voltage (0.9V/1.8V) 28 nm bulk CMOS technology is presented. A novel driver circuit is introduced for the generation of high-voltages (up to 6V) across the DEP electrodes to create strong electric fields (~10^5 V/m) for single cell manipulation. Successful integration of high voltage operation DEP electrodes with mmWave sensors, operating at 110 GHz is demonstrated. A packaging technique for integrating microfluidics with positive DEP (pDEP) on the chip for precise sample positioning and therefore optimal sensing is presented.

INTRODUCTION

Chip-scale sensors enable single cells to be studied with unprecedented sensitivity for impedance characterization [1] and flow cytometry [2]. They are also particularly useful for identifying and studying cancer cells in the absence of heterogeneous bulk tissue. mmWaves are able to bypass cell membrane and uniquely interrogate the intracellular content making them a powerful choice for single cell sensing and characterization. Moreover, Tumor Treating Fields (TTF), where electromagnetic (EM) fields are used to hinder the tumor growth, have recently gained attention as a new cancer therapy method [3]. However, the interaction of cancer cells and EM fields are poorly understood which calls for creation of platforms capable of capturing, stimulating and sensing single cells under a controlled EM environment.

High speed transistors in deep submicron CMOS technologies enable realization of high frequency sensing platforms. Moreover, fine feature sizes in these technologies allow implementation of sensing elements on the order, or smaller than, cells themselves which makes these technologies ideal for single cell interrogation. Nonetheless, high frequency sensing with extremely localized EM fields requires precise cell placement on the sensing elements. In this work microfluidics sample delivery in conjunction with on-chip generated DEP forces are employed for precise single cell positioning on a mmWave permittivity sensor to achieve optimal sensing.

SENSOR OPERATION

The sensor core consists of a mmWave ring resonator tuned at 110GHz. When operating at its fundamental mode, this resonator can be simply modeled by an inductor, L, in parallel with a capacitor, C. Therefore the resonance frequency can be calculated from:

$$\omega_{res} = \frac{1}{\sqrt{LC}} \tag{1}$$

The resonator is realized on the outermost metal layer of the chip and is thus capable of sensing permittivity changes when exposed to a given sample. A change in the permittivity of the material above the resonator introduces a shift in C, denoted by ΔC, given by [2]:

$$\Delta C = 4\pi\varepsilon_m R^3 Re\{CM^*\}\frac{|E|^2}{V^2} \tag{2}$$

where ε_m is dielectric constant of the media, R is the sample radius, E is the electric field around the electrode, V is the voltage across the electrodes, and CM represents the Clausius-Mossotti factor given by:

$$CM = (\hat{\varepsilon}_p - \hat{\varepsilon}_m)/(\hat{\varepsilon}_p + 2\hat{\varepsilon}_m) \tag{3}$$

where $\hat{\varepsilon}_p$ and $\hat{\varepsilon}_m$ are the complex permittivities of the sample and media, respectively. Equation (2) suggests that replacing the background media with the sample in locations where the electric fields are stronger, results in a larger ΔC. Therefore, in order to achieve maximum sensitivity, cells should be positioned on the resonator gap, where the E field is the largest.

By taking the derivative of Equation (1), with respect to ΔC, the corresponding shift in the resonance frequency is given by:

$$\Delta\omega_{res} = -\frac{\Delta C}{2C}\omega_{res} \tag{4}$$

In addition to aforementioned benefits of mmWave sensing, Equation (4) suggests that operating at higher frequencies enhances the sensitivity of the sensor. However, in order to operate at high frequencies, the physical dimensions of the resonator cannot be large which leads to a confinement of the fields to a very small area. This further emphasizes the need for a mechanism for precise positioning of the cells on the sensor for maximizing the performance.

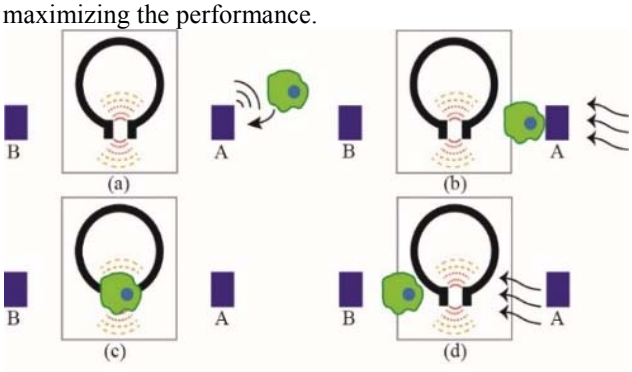

Figure 1: (a) Cell capture via DEP, (b) flow moves the cell to sensor, (c) measurement, (d) cell is removed.

Figure 1 shows the capture and measurement mechanism used in this work. DEP electrodes (A/B) attract the cell to the surface of the chip and align it with the sensing resonator. This attraction and alignment step removes the measurement dependency on both lateral position and the altitude of the cell in the channel. The channel flow moves the sample to the resonator gap, where the measurement takes place. Once the cell measurement is complete, DEP is turned off and the background flow removes the cell from the sensor.

The sensor detector circuit consists of two injection-locked oscillators operating at ω_{res}, one serving as the reference and the other as the sensor. The reference resonator is covered and therefore is not exposed to the sample. The injection-locking mechanism translates the shift in the resonance frequency of the sensing oscillator, $\Delta\omega_{res}$, due to the sample, to a phase shift, which is detected by an integrated detector consisting of mixers and amplifiers.

DEP DESIGN CONSIDERATIONS

The time-average DEP force on a particle in a media of different polarizability is given by [4]:

$$\langle F_{DEP} \rangle = 2\pi\varepsilon_m R^3 Re\{CM^*\}\nabla E^2 \qquad (5)$$

Substituting $\hat{\varepsilon} = \varepsilon - j\sigma/\omega$ in (5), the real part of CM can be calculated from:

$$Re\{CM^*\} = \frac{(\varepsilon_p-\varepsilon_m)(\varepsilon_p+2\varepsilon_m)+\frac{(\sigma_p-\sigma_m)(\sigma_p+2\sigma_m)}{\omega^2}}{(\varepsilon_p+2\varepsilon_m)^2+\left(\frac{\sigma_p+2\sigma_m}{\omega}\right)^2} \qquad (6)$$

which suggests that making $\sigma_m \ll \sigma_p$, by using a low conductivity media and working at relatively low frequencies, $Re\{CM^*\} \approx \frac{\sigma_p-\sigma_m}{\sigma_p+2\sigma_m} > 0$, thus achieving positive DEP.

The DEP electrode integration with the highly sensitive mmWave resonator is of paramount importance due to the following.

Electric Field Distribution

Figure 2 illustrates the distribution of the electric field around the resonator for two different spacings between the resonator and the DEP electrodes using a 3D EM solver, Ansoft HFSS. Comparing Figure 2(a) and (b) depicts a disturbance and leakage of the E field to the electrodes as their distance to the resonator decreases. To further illustrate this problem, the maximum E field on the resonator gap as a function of electrodes distance to the resonator is plotted in Figure 3 (dotted line). A 12% reduction in the fields is observed for the simulated distances, which suggests a lower sensitivity.

Resonator Quality Factor

The quality factor (Q) of the resonator also plays an important role in the sensitivity and the overall performance of the sensor. Figure 3 (solid line) depicts the quality factor of the resonator at 110GHz as a function of DEP electrode spacing to the resonator. The DEP electrodes in operation can be modeled by a capacitor in series with a large resistance due to routing wires, resulting in a low Q capacitor. When these electrodes are placed too close to the resonator, the capacitive coupling to the low Q capacitor causes the overall Q of the resonator to drop by up to 10%, as suggested by the simulations.

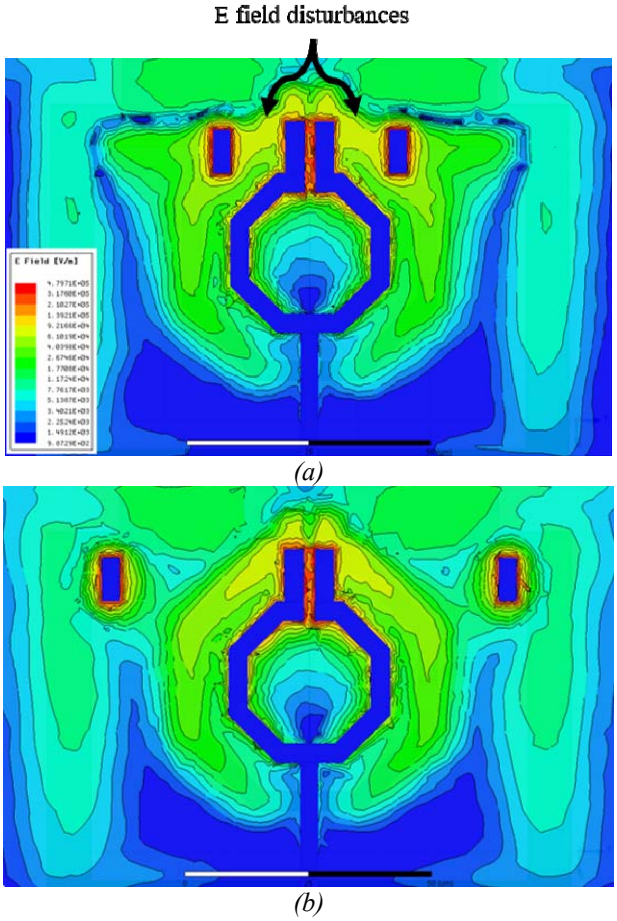

Figure 2: Electrode placement: (a) E field leakage due to close proximity of DEP electrodes, (b) minimal disturbance.

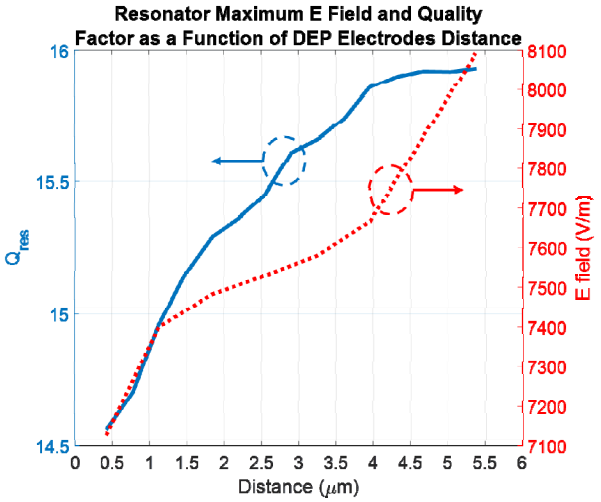

Figure 3: The effect of DEP electrodes distance to the resonator on the resonator maximum generated E field and its quality factor.

DEP DRIVER

The requisite strong fringing E-fields (~10^5V/m) for DEP manipulation are created using a combination of the proposed high voltage level generator, depicted in Figure 4(a), and steep field gradients around the DEP electrodes. Voltages exceeding device ratings are generated through stacking 1.8V-IO devices and dynamically biasing them to ensure V_{GS}, V_{DS} and V_{DG} of each transistor never exceeds the device breakdown voltage. This circuit boosts an incoming 1.8V square wave signal up to 6V (nominal 5.4V). An on-chip charge pump generates the intermediate signal levels (1.8V-3.6V) from the input. This signal is required for the dynamic biasing of the middle NMOS and PMOS transistors. The top cross coupled PMOS pair generates the other (3.6V-5.4V) level signal obviating the need for a second charge pump.

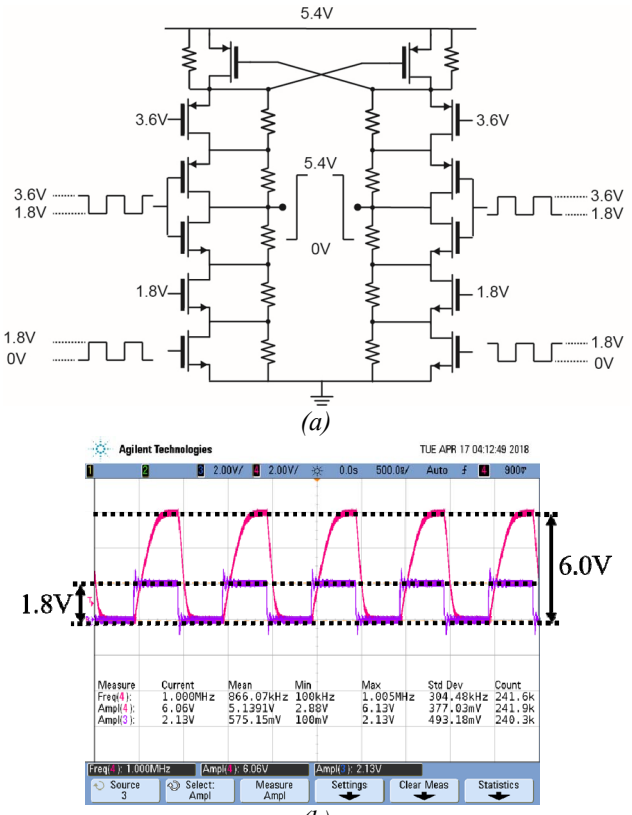

Figure 4: (a) DEP high-voltage driver, (b) input and measured output waveforms.

Each generator drives a pair of DEP electrodes and can be turned ON and OFF by disabling the 1.8V input square wave, which disables the charge pump and freezes the outputs to 0V and 5.4V. As the electrodes are covered by a thin passivation layer, no electrolysis occurs when the drivers are disabled. Alternatively, by setting the DEP frequency to somewhere close to the cross over frequency, where $Re\{CM\} \approx 0$, DEP force becomes negligible even if the generator is still operating.

Figure 4(b) shows the measurement results of boosting a 1.8V input square wave to a 6.0V output signal at 1MHz. The slow edges of the output are due to the excess loading of the chip pads, PCB traces, and oscilloscope probes that were used for measurements. In normal operation the driver is only loaded with the on-chip electrodes, with negligible capacitance, allowing a much higher operating frequency.

MICROFLUIDIC INTEGRATION

The microfluidic packaging should interface the small footprint CMOS chip (2mm x 1mm), while providing inlets and outlets for continuous sample delivery. The microfluidic channel needs to be aligned with the sensing resonator and DEP electrodes perfectly. In addition, as the chips are already diced by the foundry, they should be processed and packaged individually.

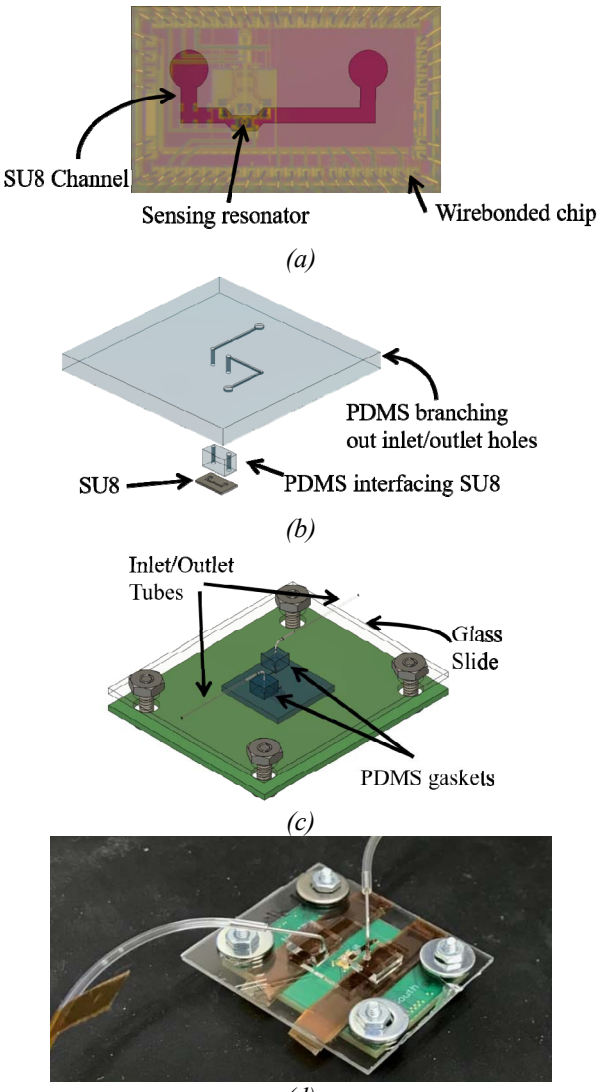

Figure 5: (a) SU8 channel, (b) various levels of the package, (c) package inlet and outlet connections, (d) complete packaged chip.

In this work, a stack of SU8, two layers of PDMS and a glass slide are used for packaging. First, chips are mounted on a glass slide and spin coated with SU8 3050, MicroChem Corp., to achieve a 50um thick layer of the resist. A chrome mask is used to pattern the channel on the SU8 as shown in Fig 5(a). Using SU8 enables creating high resolution channel structures with accurate alignment with

the sensing resonator and DEP electrodes. In addition to the channel, bond pads are exposed for chip on board connections. Next, the patterned chips are wirebonded to Printed Circuit Boards (PCB). These boards are used to power up and communicate with the chip. The first layer of PDMS is about the same size of the SU8 layer and contains two holes aligned with on chip channel holes and covers the SU8 channel which is open from the top. This layer is thicker than the height of the wirebonds so that the higher levels of the package make no contact with the wirebonds.

The second PDMS layer branches out the chip level inlet and outlet holes by forming a channel with a glass slide, as shown in Figure 5(b). Small holes are drilled on the glass slide and two thick PDMS gaskets are bonded to it in order to provide mechanical support for the tubes connected to a syringe on the inlet side and to a waste container on the output side, as shown in Figure 5(c).

All PDMS and glass surfaces are bonded together with O_2 plasma treatment. The PDMS and glass stack is screwed to the PCB and by applying mechanical pressure the PDMS and SU8 interface is sealed. Spacers on the PCB provide some support for the second layer PDMS and help in evenly distributing the mechanical force between PDMS and SU8. The complete packaged chip on the board is shown in Figure 5(d).

EXPERIMENTAL RESULTS

To enable pDEP, a low conductivity buffer was prepared (8.5% Sucrose and 0.3% Dextrose in ddH2O) [5]. A sample of HeLa GFP cells, 3e5/mL, was resuspended in the low conductivity buffer. The sample was injected into the microfluidic channel while the test chip was monitored under a fluorescence microscope. Figure 6 shows a single cell captured by a DEP electrode in alignment with the sensing resonator and is subsequently measured by the sensor. The DEP operation frequency was set to 20MHz.

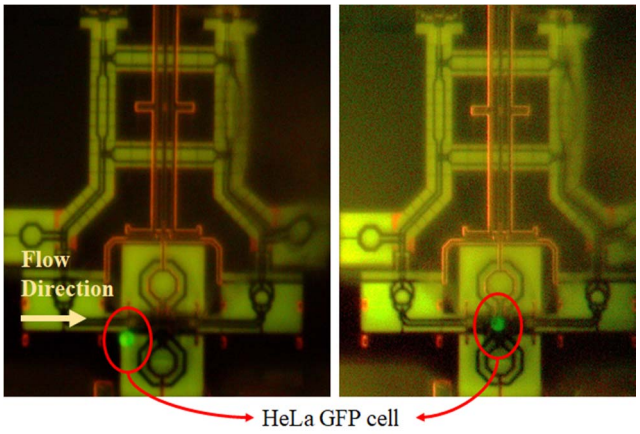

Figure 6: HeLa GFP cell trap and measurement.

To emphasize the importance of the capture and measure mechanism, the sensor signal is recorded as cells flow by for two cases with DEP ON and OFF. As shown in Figure 7, when DEP is OFF the cell inside the channel might be far away from the resonator, in both vertical and horizontal directions, and therefore the sensor is incapable of detecting the cell. However, with DEP activated a strong signal is observed at the output.

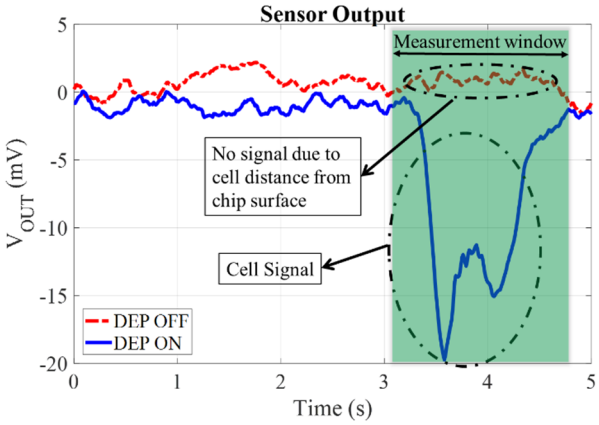

Figure 7: Sensor output with DEP ON and OFF.

CONCLUSION

In this work a DEP-assisted mmWave single-cell sensor was realized on a CMOS chip. The mmWave sensor uses a ring resonator as the sensing element, which achieves a very high sensitivity given the cells are positioned precisely on the sensing locations. DEP electrodes were designed and co-simulated with the mmWave resonator using EM tools to ensure that there are no adverse effects on the sensor performance due to proximy effects. A combination of DEP and microfluidics were employed to focus the cells on the desired location and realize a capture and measure mechanism.

AKNOWLEDGMENTS

The authors wish to thank Dr. Jun-Chau Chien and Paul Lum for technical discussions, NSF for financial support, and TSMC for chip fabrication.

REFERENCES:

[1] J.-L. Hong, K.-C. Lan, L.-S. Jang, "Electrical characteristics analysis of various cancer cells using a microfluidic device based on single-cell impedance measurement", Sensors and Actuators B: Chemical, 173 (2012), pp. 927-934.

[2] J.-C. Chien, A. Ameri, E.-C. Yeh, A.N. Killilea, M. Anwar, A.M. Niknejad, "A high-throughput flow cytometry-on-a-CMOS platform for single-cell dielectric spectroscopy at microwave frequencies", Lab on a Chip, 18 (2018), pp. 2065-2076.

[3] R. Stupp, et al., "Maintenance Therapy With Tumor-Treating Fields Plus Temozolomide vs Temozolomide Alone for Glioblastoma: A Randomized Clinical Trial", Jama, 314(23), (2015), pp. 2535-2543.

[4] R. Pethig, "Review article-dielectrophoresis: status of the theory, technology, and applications", Biomicrofluidics. 4, 2 (2015).

[5] C.-T. Ho, et al., "Rapid heterogeneous liver-cell on-chip patterning via the enhanced field-induced dielectrophoresis trap", Lab on a Chip, 6 (2006), pp. 724-736.